

## Chapter VI. Cylindrical Geometry

### 6.1 Introduction and Motivation

Understanding the principles of electrokinetics is useful for design and operation purposes of a variety of important processes. In the area of electrophoresis, most of the earlier applications of electrokinetic phenomena are fairly well understood. For instance, it is very well known that a combination of different transport driving forces is responsible for the motion of solute through a capillary channel. Although the movement of the solute species is the most important result, it can be caused by different mechanisms and not necessarily by electrophoresis which is characteristic of separation processes. On the contrary, environmental applications in porous media, for example, are mostly characterized by electroosmosis and electromigration as driving mechanisms. For simplicity, the way in which these mechanisms collaborate with other driving forces, i.e. buoyancy and hydrodynamics, has been either ignored or neglected as it is a usual practice in separation processes. The nature of soil remediation, in the domain of microfluidics, calls for a different approach where the competition among buoyancy, hydrodynamics and electroosmosis/electromigration may promote distinct flow regimes and, therefore, affect solute transport. In the previous chapter, these hydrodynamics aspects were demonstrated and reported using a rectangular geometry to represent a capillary channel.

From a practical point of view, it seems that there is insufficient theoretical analysis as to understand how to avoid the pitfalls of electrokinetic field testing. For this reason and despite the number of applications that can be listed, the applied electrical field technologies have remained non-spread (U.S. EPA, 2000). The lack of understanding of key elements for a proper design may lead to considerably impact on the movement of ions and, therefore, the

efficiency of removal of the pollutant from the contaminated soil. In particular, the determination of the optimal current density in the soil sample is an issue that also needs to be better understood as well as how it affects hydrodynamics, mass and heat transfer. Although the basic equations for the transport of solutes under an applied electrical field are known in the literature (Russel et al, 1989), it is the systematic analysis of the different effects and parameter ranges that is still missing. The analysis performed in Chapter V, based on the literature review, is the first and latest effort to provide design criteria for the different electrokinetics applications involving the three, previously mentioned, main driving forces. This initial systematic analysis was done using a rectangular geometry which can result in somewhat unrealistic findings for a porous media; however, the residual unfolded knowledge can be seen as an approximation of a capillary system. Consequently, the next logical step should be the analysis of the same driving forces in a more realistic geometry, i.e. a cylindrical capillary system.

This present chapter follows closely the approach presented in Chapter V and focuses on the analysis of the combined influence of Joule heating generation with electroosmosis and under the action of a pressure gradient. The analysis is based on the application of the fundamental equations of electrokinetic transport to determine *a priori* design criteria and apply these to show the effect of key parameters in controlling flow behavior. The goal here is rather modest and it seeks the understanding of the different flow regimes that may be possible in a cylindrical channel.

## 6.2 Model Formulation

The system been analyzed consists of a cylindrical channel of length  $L$ , radius  $R$  and an inclination of an angle  $\alpha$  with respect to the horizontal line, described in figure 6.1. The channel is exposed to a constant electrical field  $E$ . The wall of the channel, the mantle, has a net but constant and uniform charge. The wall surface presents uniform temperature as defined by its interaction with the temperature of the surroundings  $T_{\infty}$ . The axes ( $x$  and  $r$ ) have been placed coincidentally with the lower end of the capillary channel,  $x$ , and the origin of the

r-axis at the center of channel. This choice of the coordinate axis is the normal convention in cylindrical system.

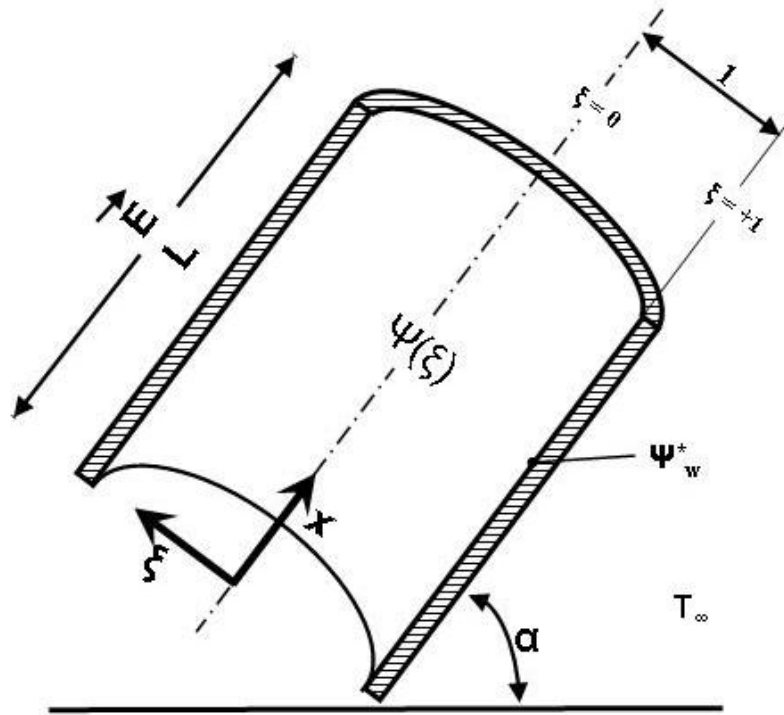


Figure 6.1 Geometrical sketch of the cylindrical capillary channel and coordinate system used in the analysis.

Modeling the system for the proposed analysis requires at least three main aspects of transport mechanism, i.e., heat transfer, electrostatics, and hydrodynamics. From the respective transport equations relevant variable profiles will be obtained for the study of the system behavior. For example, the temperature profile is originated in the heat transfer of the system interacting with its surroundings; the electrostatic potential is determined by the conservation of charge in the system stressed by electrical field and, finally, the hydrodynamics leads to the velocity profile that controls the different flows. The electrostatic model was widely discussed in Part II for this particular geometry and therefore the next sections will develop the heat transfer and the hydrodynamic models.

### 6.2.1 Heat Transfer Model

The cylindrical channel (see Figure 6.1) is assumed to interchange heat with its surroundings within a range of efficiencies, i.e., the Nusselt number may take values within a wide spectrum of possibilities. This situation may also lead to the situation in which the temperature of the wall surface of the channel at the position  $r = R$  ( $\xi = 1$ ) reach the value of temperature of its environment; this values is considered to be constant. In addition, the ratio  $R/L$  is assumed small enough to neglect any end effects on the temperature profile inside the channel. Furthermore, the conduction-dominated regime (Batchelor, 1954) is assumed valid for the present analysis. An applied electrical field  $E$  in the axial direction (i.e., the  $x$ -axis) of the channel is present and due to the fact that the fluid inside the channel shows a non-zero resistance to the electrical current, heat generation takes place. This is known as the Joule heating generation,  $Q$ , and for this study it is assumed constant with time and uniform across the channel. Under the assumptions just described, the energy equation (Bird et al., 1960) reduces to:

$$-\frac{1}{\xi} \frac{\partial}{\partial \xi} \left( \xi \frac{\partial \theta}{\partial \xi} \right) \equiv \phi^2 \quad (6.1)$$

The following definitions have been used for the non-dimensional variables:

$$\xi \equiv \frac{r}{R}; \quad \theta \equiv \frac{(T - T_\infty)}{T_\infty} \quad (6.2)$$

and the Joule heating number has been identified as:

$$\phi^2 \equiv \frac{Q R^2}{K T_\infty} \quad (6.3)$$

where,  $Q$  is the Joule heating generation,  $K$  the thermal conductivity of the fluid of the channel, and  $T_\infty$  the temperature of the surroundings of the cylindrical channel, beyond  $r = R$ .

The conservation of energy equation 6.1 needs boundary conditions at both the wall surface and the center of the cylindrical channel; although different types of boundary conditions are possible (Incropera and De Witt, 1996; Boland et al., 2000) in this analysis we are interested in a simple case. Therefore, the flux or Robin boundary conditions (Incropera and De Witt, 1996) are selected and they are given by the following equations:

$$-\left. \frac{\partial \theta}{\partial \xi} \right|_{\xi=+1} = \text{Nu} \cdot \theta \Big|_{\xi=+1} \quad @ \quad \xi = +1 \quad (6.4a)$$

$$\left. \frac{\partial \theta}{\partial \xi} \right|_{\xi=0} = 0 \quad @ \quad \xi = 0 \quad (6.4b)$$

In the previous expression, Equation (6.4a), the term Nu is the Nusselt number defined as

$$\text{Nu} \equiv \frac{h R}{K} \quad (6.5)$$

where h is the convective coefficient, R and K have been already identified above.

The solution to the differential model for the heat transfer described by equation 6.1 and boundary conditions, equation 6.4 a&b, is readily computed as:

$$\theta(\xi) = \frac{\phi^2}{4} + \frac{1}{\text{Nu}_u} \frac{\phi^2}{2} - \frac{\phi^2}{4} \xi^2 \quad (6.6)$$

Equation 6.6 is an analytical function of the position of the cylindrical channel, across radial direction, and it is very useful in the computation of the hydrodynamic velocity profile to be described in a section below. However, some interesting limiting cases can be derived

from equation 6.6 when examined. For example, the situation of a high convective cooling system, high Nusselt number values, leads to:

$$\theta(\xi) = \frac{\phi^2}{4} - \frac{\phi^2}{4} \xi^2 \quad (6.7a)$$

and for any Nusselt number value, the minimum temperature is located at the wall surface, location  $\xi=1$ , which is exposed to ambient temperature  $T_\infty$ . This is:

$$\theta_{\text{MIN}} = \frac{1}{N_u} \frac{\phi^2}{2} \quad (6.7b)$$

This situation produces the lowest temperature in the system for any value of the Joule heating parameter,  $\phi^2$ . Also, the temperature difference between any value and the lowest value is readily given by:

$$\Delta\theta(\xi) = \frac{\phi^2}{4} - \frac{\phi^2}{4} \xi^2 \quad (6.7c)$$

This equation becomes useful to predict temperature differences between the central location of the capillary channel and the surface of such domain. This is given by the following simple relation:

$$\Delta\theta(0) = \frac{\phi^2}{4} \quad (6.7d)$$

The temperature difference given by equation 6.7d depends solely on the Joule heating parameter,  $\phi^2$ . Clearly, for the case of no Joule heating generation, no temperature difference is present in the system.

## 6.2.2 Hydrodynamic Model

The fluid in the cylindrical channel, described in figure 6.1, is assumed to be Newtonian, incompressible for the mass conservation aspects and under steady state conditions. This fluid is also assumed to have constant properties everywhere except for the density in the buoyancy force term. This is, in fact, the assumption suggested by Boussinesq (Gebhart et al., 1988). All the assumptions described in section 6.2.1, above, are assumed valid for the hydrodynamic flow problem as well. In particular, the “no end effects” and the conduction-dominated regime (i.e., small magnitude of velocity field) are invoked here. Moreover, a pressure gradient is assumed to be present but its magnitude must be relatively small to comply with the assumption of a small velocity field. Under these assumptions, the axial or x-component of the Navier-Stokes equation (Bird et al., 1960) is given by

$$\frac{1}{r} \frac{\partial}{\partial r} \left( r \mu \frac{\partial V_x}{\partial r} \right) = \frac{\partial p}{\partial x} - \rho(T) g_x - \rho_e(\psi) E_x \quad (6.8)$$

where the applied electrical field in the axial direction,  $E_x$ , is assumed constant and the function  $\rho(T)$  is computed by a first order Taylor approximation around a mean temperature  $T_m$  of the system (Bird et al., 1960)

$$\rho(T) = \rho(T_m) - \beta_m \rho_m (T - T_m) \quad (6.9)$$

and where  $\beta_m$  is the volumetric compressibility of the fluid at a mean temperature  $T_m$ . Now, the parameter  $T_m$  is determined by the total mass conservation condition that may be stated as

$$2 \pi \int_0^{+R} \rho(T_m) V_x(y, T_m) r \, dr = 0 \quad (6.10a)$$

or, as a dimensionless equation

$$2 \pi \int_0^{+1} \rho_m V_x^+(\xi, \theta_m) \xi d\xi = 0 \quad (6.10b)$$

The condition given by equation 6.10 requires the computation of the hydrodynamic velocity profile previously to its solution. Finally, the function  $\rho_e$ , electrostatic density, is defined by the following expression

$$\rho_e = -\frac{\varepsilon \cdot k^2}{4 \cdot \pi} \cdot \psi(\xi) \quad (6.11)$$

where  $\varepsilon$  is the media permittivity and  $k$  is inverse of the Debye length.

As in the previous chapter, the electrostatic potential,  $\psi(\xi)$ , featuring in equation 6.11 has to be obtained by solving the Poisson-Boltzmann equation, simplified by the Debye-Huckel approximation and improved using the method proposed in chapter III, the  $f_{AO}$  correction function.

In the analysis of the velocity profile,  $V_x(r)$ , the following dimensionless variables and numbers are proposed.

$$V_E = \frac{E_x \cdot \varepsilon \cdot \psi_w}{4 \cdot \pi \cdot \mu} \quad (6.12a)$$

$$V_x^+ = \frac{V_x}{V_E} \quad (6.12b)$$

$$G_r = \frac{\beta_m \cdot \rho_m^2 \cdot B^3 \cdot T_\infty \cdot g}{\mu^2} \quad (6.12c)$$

$$G_r^* = \beta_m \cdot T_\infty \cdot G_r \quad (6.12d)$$

$$R_e = \frac{V_E \cdot B \cdot \rho_m}{\mu} \quad (6.12e)$$

$$P_m = \frac{\partial h_p}{\partial x} \cdot \frac{G_r^*}{R_e} + \sin(\alpha) \cdot \frac{G_r^*}{R_e} \quad (6.12f)$$

The Grashoff numbers, Gr and Gr\*, represent the buoyancy to viscous forces due to changes in temperature and density respectively, while in equation 6.12e, the Reynolds number, Re, represents the inertia to viscous forces. A convenient combination of Grashoff and Reynolds numbers has been mathematically applied to dimensionally reduce the total hydraulic head gradient, which yields the dimensionless number P<sub>m</sub>, equation 6.12f. By using these numbers and variables in the Navier-Stokes component, equation 6.8, the following dimensionless differential equation is obtained

$$\frac{1}{\xi} \frac{\partial}{\partial \xi} \left( \xi \frac{\partial V_x^+}{\partial \xi} \right) = P_m - \frac{Gr}{R_e} \cdot \sin(\alpha) \cdot (\theta - \theta_m) + \lambda^2 \frac{\Psi(\xi)}{\Psi_w} \quad (6.13)$$

Equation 6.13 shows several terms that account for the different forces present in the system. The left side of the equation is the viscous term, the first term on the right side represents the pressure driven force, the second is related to the buoyancy effects, and the last one is associated with the electroosmosis term.

The boundary conditions that complete the problem for the electro-hydrodynamic velocity profile are basically two. First, the maximum velocity condition will be assumed at the center of the cylindrical channel and, second, the non slip-boundary condition at the wall surface.

$$\left. \frac{\partial V_x^+}{\partial \xi} \right|_{\xi=0} = 0 \quad @ \quad \xi = 0 \quad (6.14a)$$

$$V_x^+ \Big|_{\xi=\pm 1} = 0 \quad @ \quad \xi = \pm 1 \quad (6.14b)$$

The dimensionless Navier-Stokes equation written in cylindrical coordinates, equation 6.13, can be integrated after the temperature function,  $\theta(\xi)$ , and the electrostatic potential function,  $\psi(\xi)$ , have been substituted. The solution, after applications of the boundary conditions equations 6.14 a&b have been used, yields:

$$V_x^+(\xi) = \frac{A_0}{4} \cdot (\xi^2 - 1) + \frac{A_1}{16} \cdot (\xi^4 - 1) + \left\{ 1 - \frac{I_0(\lambda\xi)}{I_0(\lambda)} \right\} \quad (6.15)$$

where, the following parameters have been identified in the function above:

$$A_0 = P_m - \frac{G_r}{R_e} \sin(\alpha) \left[ \frac{\phi^2}{4} + \frac{1}{Nu} \frac{\phi^2}{2} - \theta_m \right] \quad (6.16a)$$

$$A_1 = \frac{G_r}{R_e} \sin(\alpha) \frac{\phi^2}{4} \quad (6.16b)$$

The parameters  $A_0$  and  $A_1$  are both closely related to the buoyancy driven term and affected by the Joule heating effect. Only  $A_0$  is related to the pressure driven term. Some of the qualitative and semi-qualitative information about the flow given by the hydrodynamic velocity profile is analyzed in the section below.

### 6.2.3 The Mass Conservation Condition

After an analytical expression for the velocity profile has been determined it is introduced in the mass conservation equation (Eq. 5.10) in order to isolate the characteristic mean temperature of the system,  $T_m$ , or its equivalent dimensionless form,  $\theta_m$ . This last step constitutes the closing loop of the solution procedure for the entire system. The expression in this case corresponds to:

$$\theta_m = \frac{16 \left\{ \frac{1}{2} - \frac{I_1(\lambda)}{\lambda I_0(\lambda)} \right\} - P_m}{\frac{G_r}{R_e} \cdot \sin(\alpha)} + \frac{1}{Nu} \frac{\phi^2}{2} + \frac{\phi^2}{6} \quad (6.17)$$

Equation 6.17 is a function of the dimensionless hydraulic pressure gradient,  $P_m$ , the Nusselt number,  $Nu$ , the modified Debye length,  $\lambda$ , the Joule heating generation number,  $\phi^2$ , the inclination angle,  $\alpha$ , the Grashoff number,  $Gr$ , and Reynolds number,  $Re$ . In addition,  $\theta_m$  is a linear function of the parameter  $P_m$ , the Reynolds number,  $Re$ , and Joule heating generation,  $\phi^2$ . In contrast,  $\theta_m$  is an hyperbolic function of both the  $Nu$  and the Grashoff number,  $Gr$ , as well as of the inclination angle,  $\alpha$ . The dimensionless Debye length,  $\lambda$ , is present through a non-linear relationship.

### 6.3 Design Criteria

The temperature and velocity profiles must be found in a range of meaningful numerical values. To accomplish this, a number of new criteria must be developed by restricting the range of feasible values of those parameters affecting temperature and velocity. One of them, the Joule heating generation number,  $\phi^2$ , cannot take values that imply a change in the fluid phase. Under ambient conditions change of phase will occur at temperature values of approximately  $\theta \geq 0.28$  yielding a range of the Joule heating generation number of  $0 \leq \phi^2 \leq 0.8$ . This criterion is implicit in all the calculations herein presented. Another physical constraint taken into consideration is that the mean temperature can not exceed the maximum temperature in the system. By using this physical constraint, a range of feasible values for the dimensionless hydraulic head gradient has been derived. In particular, the system under study is symmetrical and therefore the location of maximum temperature is the center of the capillary. Equations (21a) and (21b) are used to identify its value respectively.

$$\xi_{\text{MAX}} = 0 \quad (6.18a)$$

$$\theta_{\text{MAX}} = \frac{\phi^2}{4} + \frac{1}{N_u} \frac{\phi^2}{2} \quad (6.18b)$$

Conversely, equations (6.19a) and (6.19b) are used to identify the location of minimum temperature and its value respectively.

$$\xi_{\text{MIN}} = +1 \quad (6.19a)$$

$$\theta_{\text{MIN}} = + \frac{1}{N_u} \frac{\phi^2}{2} \quad (6.19b)$$

Combining the expressions for maximum and minimum temperature in the system, equations (6.18b) and (6.19b), with the expression for the mean temperature, equation (6.17), the following dimensionless hydraulic head gradient criteria are established.

$$\text{Pm}_{\text{MIN}} = 16 \left\{ \frac{1}{2} - \frac{I_1(\lambda)}{\lambda I_0(\lambda)} \right\} - \frac{G_r}{R_e} \sin(\alpha) \frac{\phi^2}{12} \quad (6.20)$$

$$\text{Pm}_{\text{MAX}} = 16 \left\{ \frac{1}{2} - \frac{I_1(\lambda)}{\lambda I_0(\lambda)} \right\} + \frac{G_r}{R_e} \sin(\alpha) \frac{\phi^2}{6} \quad (6.21)$$

These design equations are useful to identify parameter values for the numerical illustrations that will be presented in the next section. Repeatedly, the criteria represented by equations (6.20) and (6.21) are implicit in all the calculations herein presented.

## 6.4 Illustrative Results and Discussion

Figure 6.2 (a&b) shows the temperature profile for two cases of Nusselt number with the Joule heating number,  $\phi^2$ , as a parameter ranging between the values of 0.05 and 0.80. These are the cases of Nusselt number  $Nu = 10$  (cooling system), (a), and case of Nusselt number  $Nu = 5$  (less cooling system), (b).

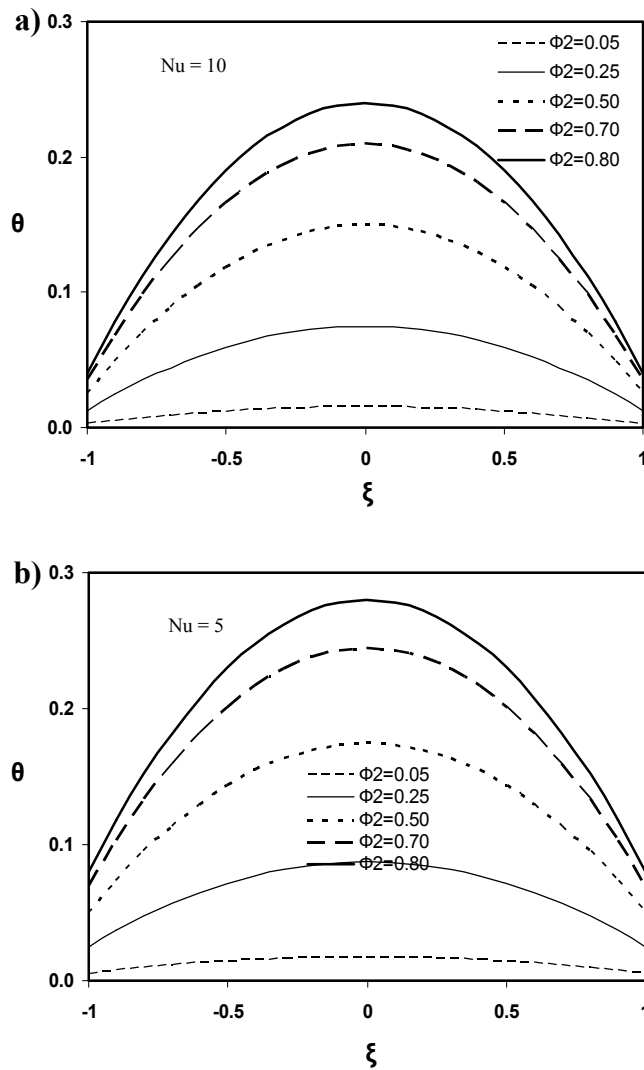


Figure 6.2 Dimensionless temperature profiles (inside a cylindrical capillary channel) for various values of the heat generation parameter.

By comparing figures 6.2a and 6.2b it is clearly observed the important role of the heat exchange forces; for example, in the case of the smaller Nusselt value there is a “lifting” effect on all the temperature values, equally distributed along the radial position  $\xi$ . Due to the symmetric characteristics of the system, the locations of maximum temperature values are found at the center of the capillary. In addition, an increase in the Joule heating parameter yields a more pronounced parabolic type curve. For example, an increment of  $\phi^2$  from 0.25 to 0.70 produces an increase in temperature of 250% at the location  $\xi=0$ . At the same location, an increment of  $\phi^2$  from 0.25 to 0.50 produces an increase in temperature of 110% and an increment of  $\phi^2$  from 0.05 to 0.25 increases temperature by 700%. This observed effect indicates that a small variation on the Joule heating parameter may cause an important impact on the system temperature specially in the lower range of  $\phi^2$ .

In order to illustrate the role of the Joule heating, the buoyancy and electroosmotic forces, and field direction on the velocity profile three sets of figures are presented and analyzed. On all these plots the dimensionless Debye length is used as a parameter between  $\lambda = 1$  and  $\lambda = 20$ . This particular range covers the most typical values of Debye lengths that have actual effect on the electrostatic potential and, therefore, on velocity.

Figure 6.3 (a,b&c) show velocity profiles for three cases of the Joule heating parameter,  $\phi^2 = 0.05$  (a),  $\phi^2 = 0.3$  (b) and  $\phi^2 = 0.8$  (c) respectively, with Debye length as a parameter with the values indicated in the figure. On this set of plots the Grashoff number has been held at the value of unity while the electrostatic field is in the axial axis direction. In figure 6.3a, it is clearly observed that at low values of  $\phi^2$  (0.05) electroosmosis dominates presenting a *flow reversal regime*. For values of  $\lambda = 1$  and  $\lambda = 2$ , this is not necessarily noticeable because of the scale used in the figure. In the next two plots, figure 6.3 (b&c), where the Joule heating parameter is gradually increased, buoyancy forces begin to compete and change the direction of flow at the center of the cylindrical capillary. The phenomenon just described caused *double flow reversal regime* of higher magnitude with higher Debye length and higher Joule heating parameter.

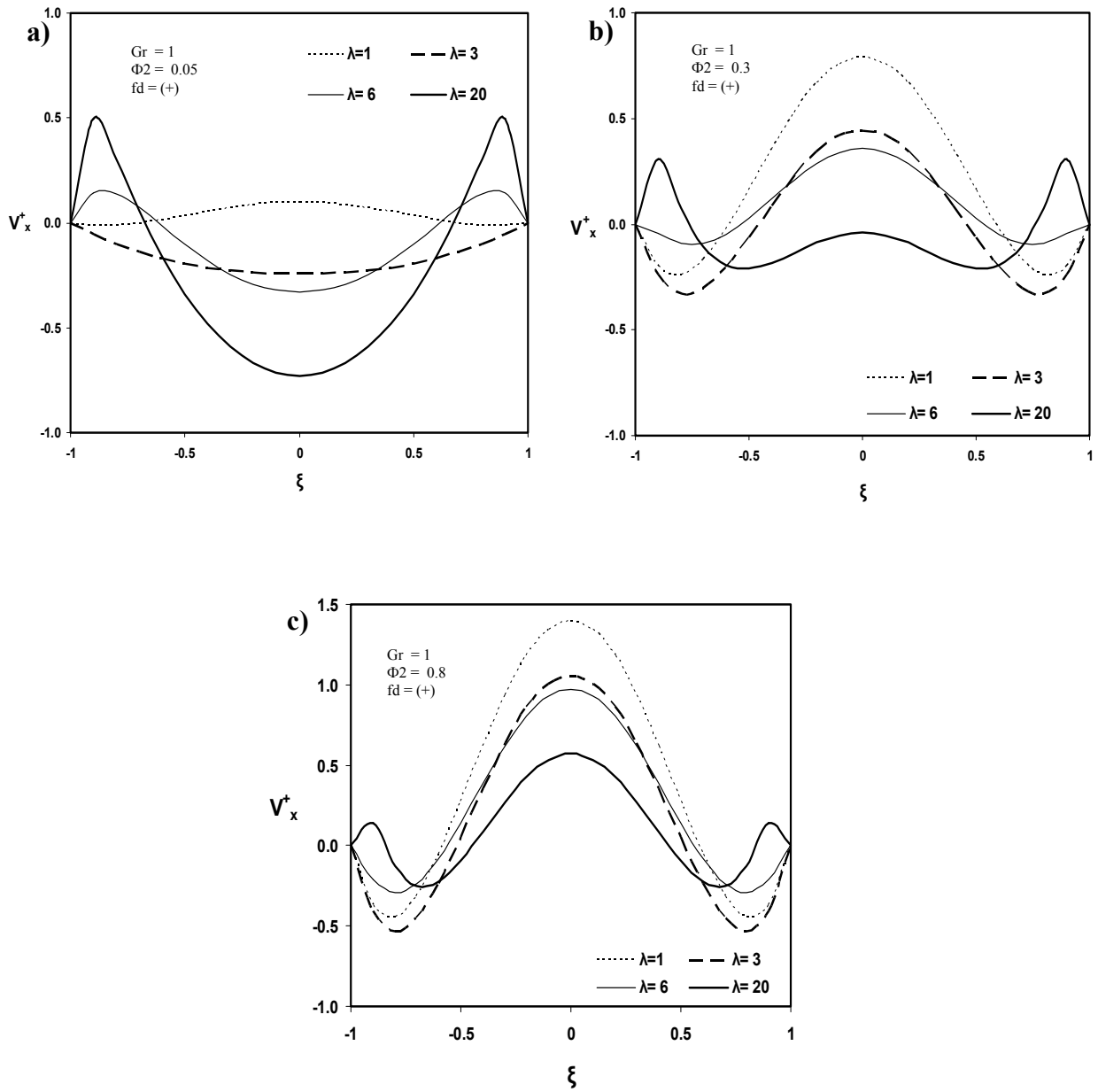


Figure 6.3 Typical hydrodynamic behavior of the physical system (inside a cylindrical capillary channel) for Grashof number  $Gr = 1$  and electrical field in the axis direction.

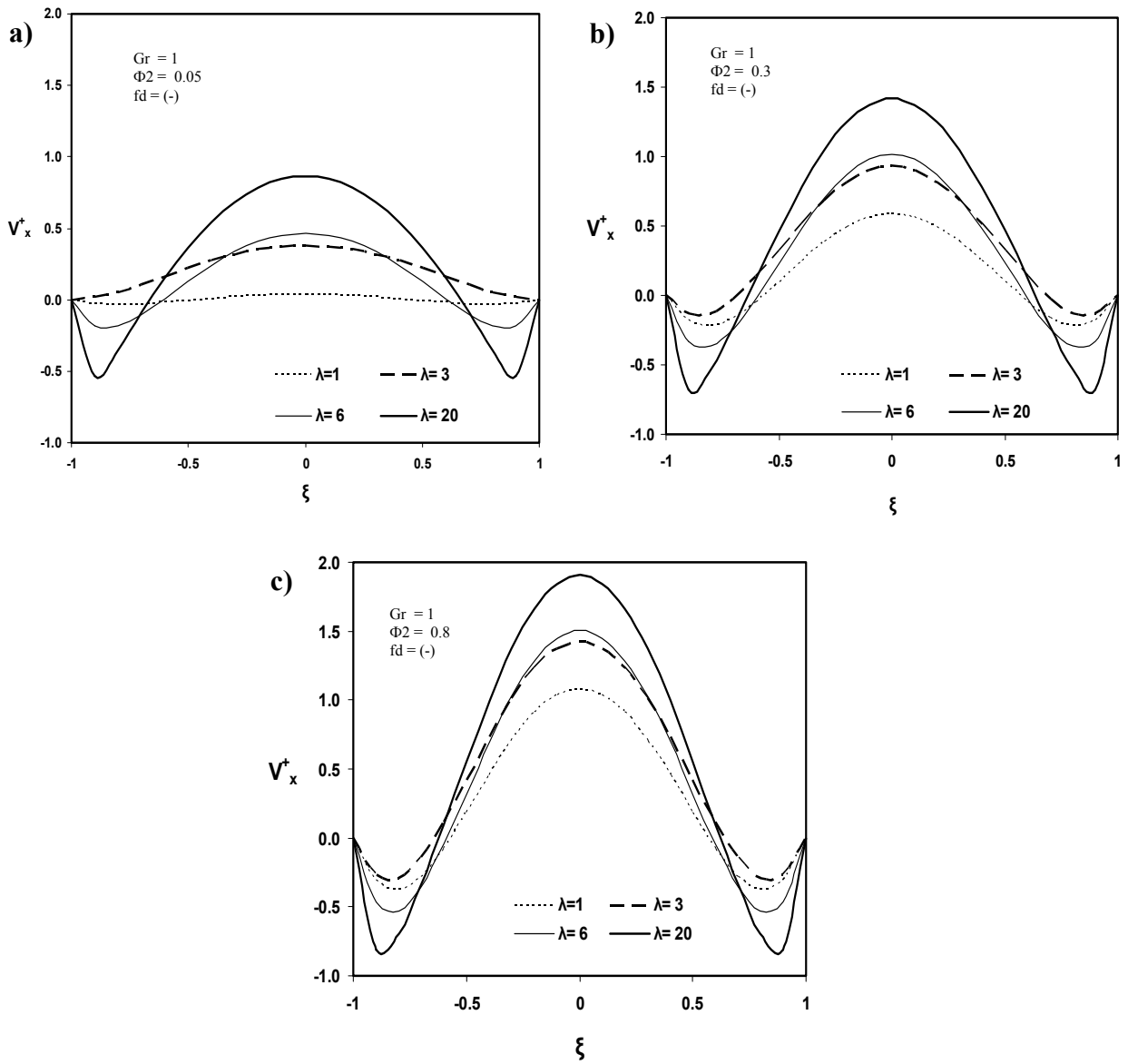


Figure 6.4 Typical hydrodynamic behavior of the physical system (inside a cylindrical capillary channel) for Grashof number  $Gr = 0.8$  and electrical field in the opposite direction of axis.

Figures 6.4 (a,b&c) describe the same variables as in figures 6.3 (a,b&c), dimensionless-axial velocity profiles inside the capillary channel for different values of the Joule heating number ( $\phi^2=0.05$  (a),  $\phi^2=0.3$  (b), and  $\phi^2=0.8$  (c)); however, inverting the electrostatic field direction. Also, the Grashoff number has been held at the value of 0.8 instead of unity for presentation purposes. In general, the set of figures shows a very well defined trend in flow regime for all the cases portrayed. For example, for low  $\lambda$  values (1 and 2) on figure 6.4a an insipient *flow reversal regime* is presented. The same trend and in a more obvious way is clearly observed at higher values of  $\lambda$  (6 and 20). Figures 6.4 b&c are an amplified version of the previous ones. Apparently electroosmosis and buoyancy are collaborating against hydraulic forces to portray flow reversals. The amplitude of the sinusoidal type of curve is higher as higher are the Debye length and the Joule heating parameter.

Figure 6.5 (a,b&c) present velocity profiles for three cases of the Joule heating parameter,  $\phi^2=0.05$  (a),  $\phi^2=0.3$  (b) and  $\phi^2=0.8$  (c) respectively, with Debye length as a parameter with the values indicated in the figure. Furthermore, figures 6.5 (a,b&c) present the same dimensionless-axial velocity profiles (inside the capillary channel) as in figures 6.3 (a,b&c); however, the effect of buoyancy has been attenuated or diminished for cases where the Grashoff number shows a lower value ( $Gr = 0.01$ ). The set of figures show only a pressure-driven and an electroosmotic-driven family of flow regimes for all values of the Joule heating generation number. In the case of low Debye length parameter  $\lambda$  values ( $<2$ ) the flow regime is pressure-driven while higher values cause *flow reversal*.

A brief summary of ideas projected from the analysis and discussion of figures 6.3 - 6.5 clearly indicates that *flow reversal* may occur under different type of scenarios. This early conclusion will be validated by the other geometrical approaches.

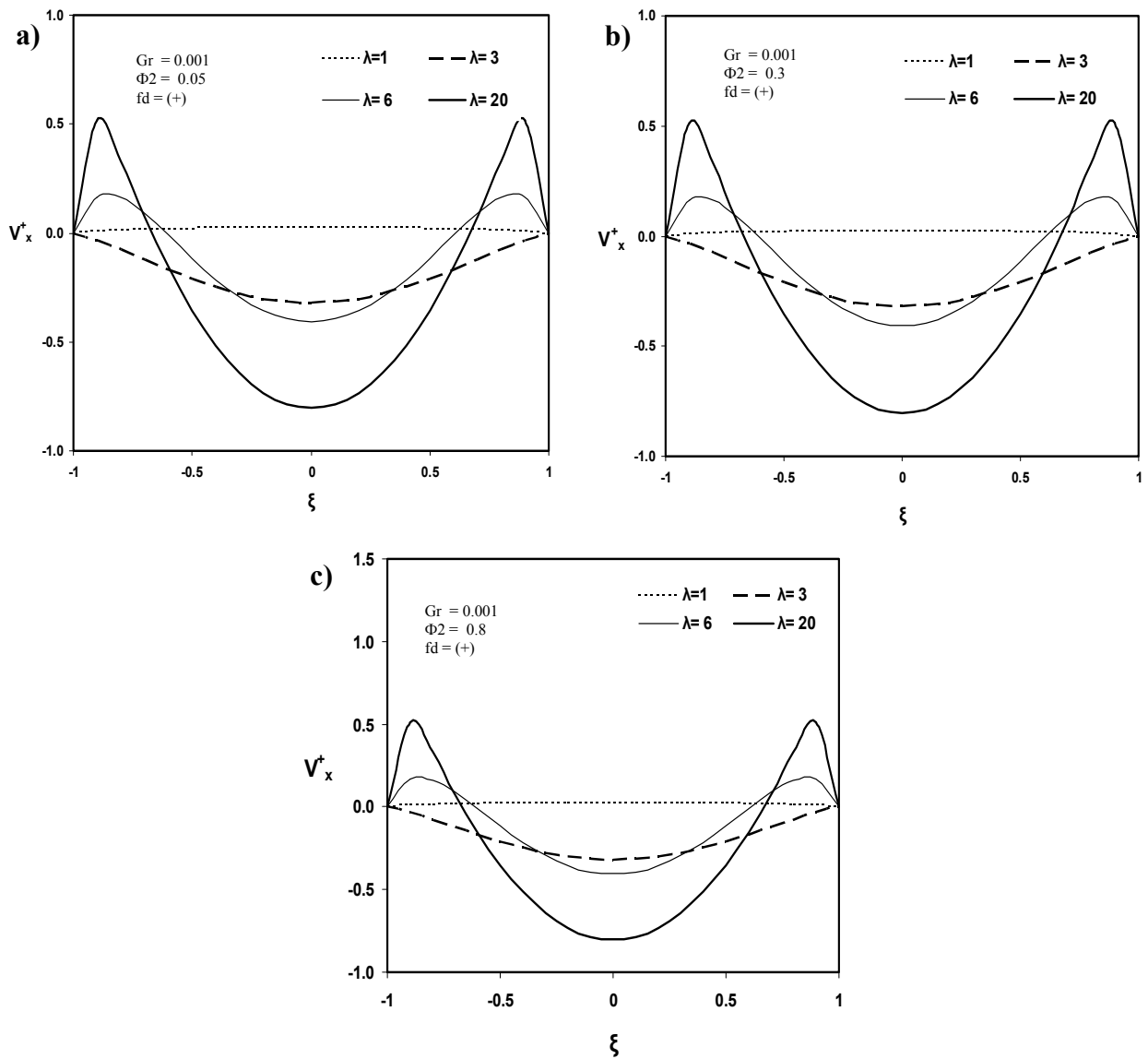


Figure 6.5 Typical hydrodynamic behavior of the physical system (inside a cylindrical capillary channel) for low influence of the buoyancy forces, Grashoff number  $Gr = 10^{-2}$  and electrical field in the axis direction.

## 6.5 Summary of the Chapter

The present chapter is the second in a series of three dedicated to study the hydrodynamic aspects involved in a capillary channel. In particular, this chapter targets the cylindrical geometry and its related issues. As in the previous chapter, porous media has been simulated using this geometry approach to determine the different effect of the three main driving forces, found in electroremediation, on flow regime. In order to capture the main fundamental principles as well as the practical aspects and its results, this chapter is presented in sections.

First, porous media may be associated more with a cylindrical geometry than with a rectangular aspect. Therefore, the interest of obtaining quantitative and semi-quantitative descriptions of the hydrodynamic has been extended to the cylindrical capillary channel. This chapter incorporates the main geometry differences into the study.

Second, the chapter describes the physical model and details of assumptions considered in a cylindrical capillary channel. Fundamental principles are presented as well as their role in the mathematical description of the system under study. For the most part, this chapter concentrates only in developing the heat transfer and Navier-Stokes equations.

Finally, a complete description of the system under study is performed via illustrative results. Portraits for different flow regimes are obtained using the analytical solution of the fundamental equations describing the cylindrical system. A comparison of driving forces is presented and the most characteristic cases are identified.